Magnonic Frequency Comb in the Magnomechanical Resonator

Guan-Ting Xu,[1,2,3,*] Mai Zhang,[1,2,3,*] Yu Wang,[1,2] Zhen Shen,[1,2,3,†] Guang-Can Guo,[1,2,3] and Chun-Hua Dong[1,2,3,‡]
[1]*CAS Key Laboratory of Quantum Information, University of Science and Technology of China, Hefei, Anhui 230026, People's Republic of China*
[2]*CAS Center for Excellence in Quantum Information and Quantum Physics, University of Science and Technology of China, Hefei, Anhui 230088, People's Republic of China*
[3]*Hefei National Laboratory, University of Science and Technology of China, Hefei, Anhui 230088, People's Republic of China*

(Received 14 May 2023; accepted 16 November 2023; published 11 December 2023)

An optical frequency comb is a spectrum of optical radiation which consists of evenly spaced and phase-coherent narrow spectral lines and is initially invented in a laser for frequency metrology purposes. A direct analog of frequency combs in the magnonic systems has not been demonstrated to date. In our experiment, we generate a new magnonic frequency comb in the resonator with giant mechanical oscillations through the magnomechanical interaction. We observe the magnonic frequency comb contains up to 20 comb lines, which are separated by the mechanical frequency of 10.08 MHz. The thermal effect based on the strong pump power induces the cyclic oscillation of the magnon frequency shift, which leads to a periodic oscillation of the magnonic frequency comb. Moreover, we demonstrate the stabilization and control of the frequency spacing of the magnonic frequency comb via injection locking. Our Letter lays the groundwork for magnonic frequency combs in the fields of sensing and metrology.

DOI: 10.1103/PhysRevLett.131.243601

Introduction.—Optical frequency combs are composed of a set of equidistant coherent optical lines in the frequency domain. In the last two decades, they have exhibited rapid development in various fields [1–3], such as astronomy and cosmology, optical atomic clock [4], light detection and ranging (LiDAR) [5–7], low-noise microwave source [8–10], coherent optical communication [11,12], quantum key distribution [13], dual-comb spectroscopy [14,15], spectrometer [16,17], and optical coherence tomography [18,19]. Optical frequency combs in microresonators can be generated through third-order Kerr nonlinearity $\chi^{(3)}$ or electro-optical modulation [2,20,21]. Recently, mechanical vibration has been demonstrated for the generation and engineering of optical combs [22–26], which has attracted increasing attention due to its low repetition rate and suitability for acoustic sensing [27]. Furthermore, the frequency combs have also been well investigated beyond optical systems, such as microwave systems and phononic systems. However, the frequency comb in the magnonic system has not been demonstrated to date.

Magnons are the quanta of collective spin excitation of magnetization in ferromagnetic insulators such as yttrium iron garnet (YIG). They exhibit great frequency tunability, extremely low magnetic damping, and high Curie temperature, making them an ideal carrier for performing coherent information processing, and precision measurements [28–34]. Similar to the traditional frequency comb, the magnonic frequency comb has been proposed for the development of high-precision magnonic frequency metrology and spectroscopy via nonlinear interaction [35–37]. However, the weak nonlinear interaction of magnons presents a challenge for generating magnonic frequency combs [38]. Recently, several research works have reported on cavity magnomechanical systems, where the magnetostrictive interaction can induce the nonlinear oscillation of the magnons within the YIG sphere [39–42]. Following the success of introducing mechanical vibration, the magnonic frequency comb based on magnetomechanical coupling has been proposed in theory [43].

In this Letter, we experimentally generate a magnonic frequency comb in the resonator with giant mechanical oscillation through the magnomechanical interaction. This dynamical process is facilitated by an external pump that enables magnomechanical interactions mediated through the magnetostrictive effect. When the pump power is strong enough, magnomechanical nonlinearities play a significant role, and a self-induced nonlinear phenomenon similar to the Kerr-frequency comb effect can be observed in the magnomechanical system. We observe a magnonic frequency comb with up to 20 comb lines and a frequency spacing of 10.08 MHz, equaling the resonant frequency of the mechanical resonator. In this process, the strong pump field on the magnon is required, leading to a raised temperature of the magnon and a corresponding magnon frequency shift. Then, the magnonic frequency comb shows periodic oscillation due to the thermal effect. It is also in good agreement with the theoretical calculation based on the evolution equations of the magnon and phonon modes. Finally, we demonstrate the stabilization

and control of the frequency spacing of the magnonic frequency comb via injection locking [44]. We can achieve tuning of comb teeth beyond a range of 1 kHz.

Experimental results.—Because of magnetostrictive forces, a type of radiation pressurelike interaction arises between the magnon mode and the mechanical mode, as shown in Fig. 1(a). When increasing the pump power to enhance the interaction, the self-induced nonlinear phenomena similar to the Kerr-frequency comb effect can be observed in the magnomechanical system based on the cascaded two-magnon process, as illustrated in Figs. 1(b) and 1(c). In this two-magnon process, two magnons

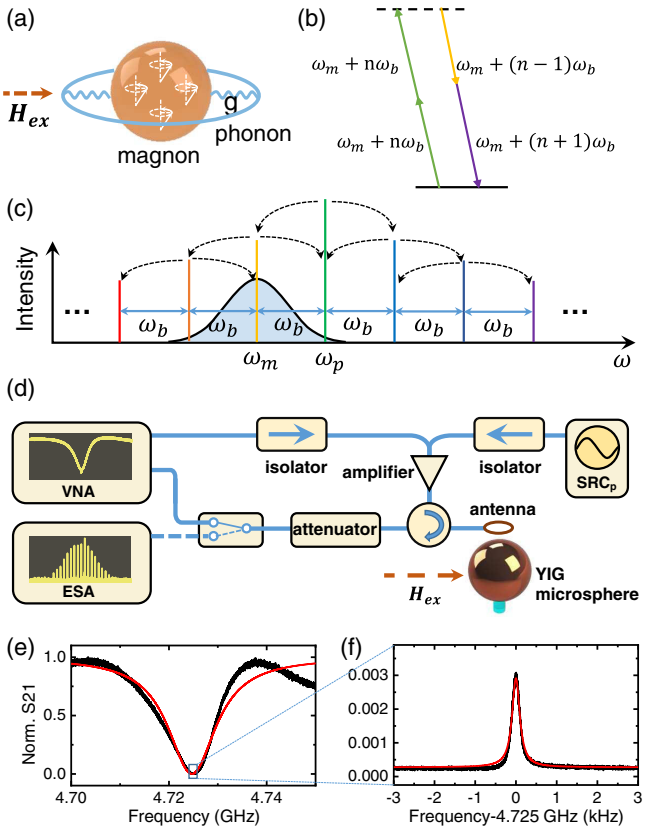

FIG. 1. (a) Illustration of the coupling between magnon and phonon with single magnon-phonon coupling strength g. (b) The magnonic frequency comb is generated via a two-magnon process. Two magnons with frequency $\omega_m + n\omega_b$ are annihilated to create two magnons with frequency $\omega_m + (n-1)\omega_b$ and $\omega_m + (n+1)\omega_b$, where the ω_m and ω_b are the frequency of the magnon and mechanical modes, respectively. (c) A cascaded two-magnon process is initiated to form a frequency comb separated with a mechanical frequency of ω_b. (d) Schematic of the experimental setup for the magnonic frequency comb. SRC: microwave source; VNA: vector network analyzer; ESA: electrical spectrum analyzer. (e) Measured microwave reflection spectrum around 4.725 GHz. (f) The detailed spectrum showing the mechanical mode in (e). The red lines are the results of theoretical calculations discussed in the main text with the parameters of $g/2\pi = 2.36$ mHz, $\kappa_m/2\pi = 12$ MHz, $\kappa_b/2\pi = 220$ Hz, and $\kappa_{\rm in}/2\pi = 6.1$ MHz.

with the frequency of $\omega_m + n\omega_b$ are annihilated to create two magnons with frequency $\omega_m + (n-1)\omega_b$ and $\omega_m + (n+1)\omega_b$, where the ω_m and ω_b are the frequency of the magnon and mechanical modes, respectively. This initiates a cascaded process leading to the formation of a frequency comb with a free spacing of ω_b; the frequency relationship between the magnon frequency ω_m, mechanical frequency ω_b, and pump frequency ω_p is given by $\omega_m = \omega_p - \omega_b$. The interaction between the magnon and mechanical modes can be represented by the Hamiltonian expression:

$$H/\hbar = (\omega_m - \omega_p)m^\dagger m + \omega_b b^\dagger b + g(b^\dagger + b)m^\dagger m + i\sqrt{\kappa_{\rm in}}\varepsilon_p(m^\dagger - m) \quad (1)$$

where m and b are the annihilation operators of the magnon and mechanical modes, κ_m and κ_b represent the dissipation rate of magnon and phonon, respectively. g is the single magnon-phonon coupling strength, which depends on the overlap between magnon and phonon modes. ε_p is the pump field of the microwave with the frequency of ω_p. $\kappa_{\rm in}$ is the input coupling rate of the microwave. For the blue-detuned pump, the relationship between ω_m and ω_b satisfies $\Delta = \omega_p - \omega_m = \omega_b$.

As shown in the Hamiltonian, coupling between magnons and phonons leads to the phonon-number dependent magnon frequency shift:

$$\frac{dm}{dt} = \left\{ i[\Delta - g(b^\dagger + b)] - \frac{\kappa_m}{2} \right\} m + \sqrt{\kappa_{\rm in}}\varepsilon_p, \quad (2)$$

$$\frac{db}{dt} = \left(-i\omega_b - \frac{\kappa_b}{2} \right) b - igm^\dagger m. \quad (3)$$

Like the frequency comb induced by the Kerr oscillator, when the pump condition exceeds a threshold, there will be mechanical parametric instability in the system [40,41]. Modulated by the strongly excited mechanical mode, the magnon comb generates, where the amplitude of magnon mode will take a form as $m(t) = \sum_n m_n e^{in\omega_b t}$, $n \in Z$, where $m_n = i^n \sqrt{\kappa_{\rm in}}\varepsilon_p \sum_k \{J_{n-k}(\xi)J_n(-\xi)/[\kappa_m/2 - i(\Delta + k\omega_b)]\}$ and $\xi = 2g|b|/\omega_b$ is the normalized amplitude of mechanical mode. Meanwhile, the linewidth of the mechanical mode is also narrowed significantly by the magnon comb that $\kappa_b' = \kappa_b - \chi$. As the narrow linewidth of the mechanical mode, the no-coherence part of the magnon pump can be ignored and there is $\chi = 2g\sum_n {\rm Im}[m_n^\dagger m_{n+1}]/|b|$. When $\kappa_b' \le 0$, the system is unstable and a magnon comb occurs (see Supplemental Material [45] for more details).

The experiment setup is illustrated in Fig. 1(d). Initially, a YIG microsphere with a diameter of 623.6 μm is subject to a bias magnetic field H_{ex} aligned parallel to the equatorial plane of the YIG microsphere, which supports a uniform magnon mode. The relation between the frequency of

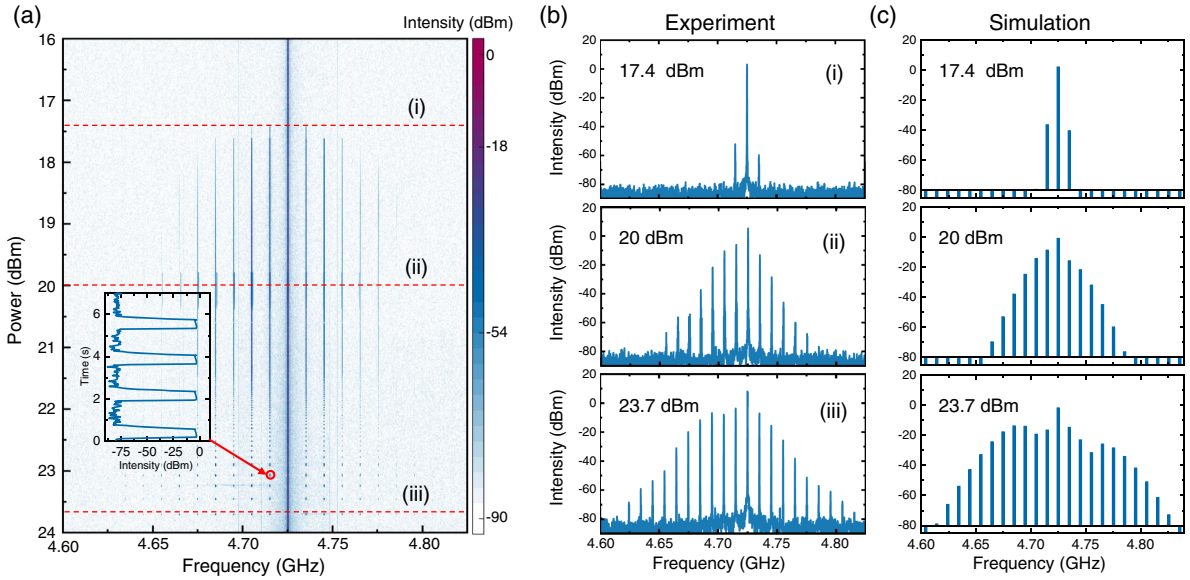

FIG. 2. (a) Evolution of the magnonic frequency comb along increased pump power from 16 to 24 dBm with the frequency of $\omega_p = 4.725$ GHz. Inset: evolution of the spectrum over a period of 7 s at a power of 23.1 dBm and frequency $\omega_p - \omega_b = 4.714$ GHz component. (b) Snapshots with different evolution stages in (a). (c) Simulated spectra of the magnonic frequency combs with the same conditions in (b).

the magnon and magnetic field intensity follows the equation $\omega_m = \gamma H_{ex}$, where $\gamma = 2\pi \times 2.8$ MHz/Oe represents the gyromagnetic ratio. In order to excite the magnon mode, we employ an antenna located close to the YIG microsphere with a frequency of around 4.725 GHz. Figure 1(e) shows the magnon resonance with a dissipation rate of $\kappa_m/2\pi = 12$ MHz through the microwave reflection spectrum S_{21} obtained by a vector network analyzer (VNA), corresponding to the Q factor of 394. The frequency associated with the mechanical mode is obtained as $\omega_b/2\pi = 10.08$ MHz [33,46]. The dissipation rate of the mechanical mode is $\kappa_b/2\pi = 220$ Hz, as shown in Fig. 1(f). The Q factor of the mechanical mode is 46 000. Meanwhile the pump field of the microwave has frequency of $\omega_p = 4.725$ GHz. Based on these interactions, the theoretical calculations are achieved with the parameter of the single magnon-phonon coupling strength $g/2\pi = 2.36$ mHz and the input coupling rate of microwave $\kappa_{\text{in}}/2\pi = 6.1$ MHz.

Figure 2 displays the spectra of the magnonic frequency comb with varying pump power from 16 to 24 dBm at the frequency of $\omega_p = 4.725$ GHz. For a weak microwave pump field, i.e., below the threshold of 17.4 dBm, the spectrum only contains the pump component, with no comb lines. As the pump power gradually increases to reach the threshold for generating comb conditions, a frequency comb emerges, as shown in Fig. 2(b), with a tooth spacing of $\omega_b = 10.08$ MHz. The number of comb lines increases steadily with higher pump power. The typical magnonic frequency comb can have up to 21 comb lines with the pump power at 23.7 dBm. Figure 2(c) displays magnonic frequency combs obtained from numerical simulations of the dynamics equations under the pump power of 17.4 dBm, 20 dBm, and 23.6 dBm, respectively. Since a strong pump heats the system, the magnon mode is redshifted due to the thermal effect, and the effective detuning between pump frequency and magnon frequency $\Delta\omega_{\text{eff}}$ are $1.1\omega_b$, $1.3\omega_b$, and $2\omega_b$, respectively. These inconsistent detunings are mainly caused by thermal effects, which we will discuss later. Other numerical simulation parameters are consistent with the experiment.

During the process of increasing pump power, it is observed that when the pump power reaches 21.4 dBm, the comb teeth become unstable and oscillate in the time domain, with the oscillation period increases as the power increases. The inset of Fig. 2(a) shows the evolution of a typical comb line over a period of 7 s at a power of 23.1 dBm at a frequency of $\omega_p - \omega_b = 4.714$ GHz. To investigate the physical mechanism for this oscillation, we further investigate the dynamic evolution of the magnon mode. When we fix the pump frequency at $\omega_p = 4.725$ GHz and the power at 23.1 dBm, we observe the temporal evolution of the S_{21} spectrum measured by a VNA, as shown in Fig. 3(a). The comb generation exhibits a periodicity of $T = 1.7$ s, corresponding to the period shown in the inset of Fig. 2(a). Figures 3(b) and 3(c) show the typical S_{21} spectrum at $t = 2$ s and 3 s in Fig. 3(a), respectively. When the pump power is very strong, an artifact signal peak will appear at the overlap of the comb tooth frequency (4.714 GHz) in the S_{21} spectrum, and its frequency is related to the resolution bandwidth of the VNA. In addition, the oscillation time scale is similar to that

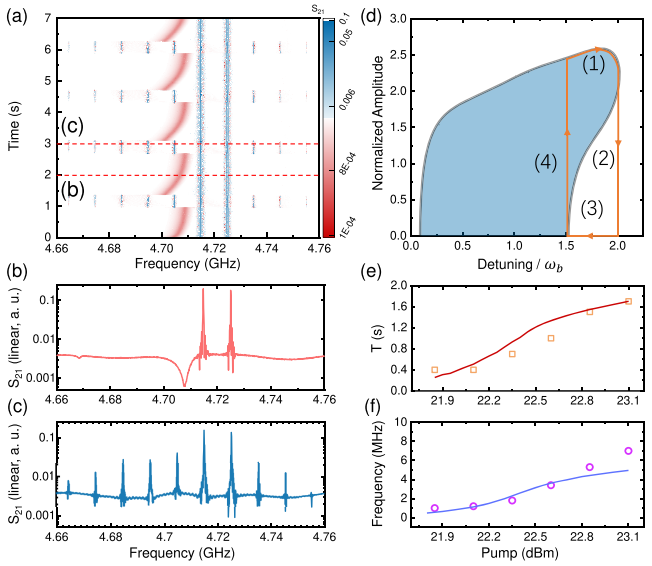

FIG. 3. (a) Evolution of the S_{21} spectrum along time (within 7 s) with the pump power of 23.1 dBm and frequency of $\omega_p = 4.725$ GHz. (b),(c) The typical S_{21} spectrum under $t = 2$ s and 3 s in (a). (d) Threshold curve for phonon amplitude and detuning at the pump power of 23.1 dBm. (e),(f) The oscillation period and the frequency shift versus pump power from 21.85 to 23.1 dBm. The solid line is the theoretical curve.

of thermal relaxation [26,47]. We conduct further analysis to investigate the thermal effect during tooth generation. With a large amount of energy coupled into the system, the YIG sphere will be heated:

$$\frac{d\delta T}{dt} = -\frac{1}{\tau}\delta T + \frac{\kappa_{\text{in}}\hbar\omega_p m^\dagger m}{c_p}, \tag{4}$$

where δT is the temperature difference between YIG and the environment, $\tau = 1.6$ s is the thermal relaxation time, $c_p = 9.55 \times 10^{-3}$ J/K is the thermal capacity of the YIG sphere, and $\kappa_{\text{in}} = \kappa_m - \kappa_{ex}$ is the intrinsic dissipation rate. As a result, the frequency of the magnon mode will be redshifted with the increasing temperature:

$$\omega_m' = \omega_m - \alpha_{\text{T}}(\delta T - \delta T_0), \tag{5}$$

where $\alpha_{\text{T}} = 0.41$ MHz/K is the frequency shift per unit temperature change and $\delta T_0 = 4.2$ K is the initial temperature difference. Figure 3(d) depicts the threshold curve of phonon amplitude versus detuning, where $\kappa_b' = 0$. Points on the curve indicate steady states. For states under the curve corresponding to the shaded fill area in Fig. 3(d), there is $\kappa_b' < 0$ and phonon amplitude will increase. Conversely, for states above the curve corresponding to the blank space in Fig. 3(d), there is $\kappa_b' > 0$ and the phonon amplitude will decrease. Moreover, as shown in Fig. 3(d), this process can be divided into four processes: (1) When the threshold is approached, a large number of magnons are generated, causing the YIG sphere to heat up and leading to a redshift in the magnon frequency due to thermal effects. (2) When the frequency shift is substantial enough, the threshold cannot be approached for all amplitudes of the mechanical mode. At this time, the magnon number will dramatically decrease due to the large detuning between resonances. (3) The YIG sphere will no longer heat up, and the heat will be dissipated into the ambient air, causing the magnon frequency to shift back in the direction of high frequency. (4) If the pump power remains constant, the magnon frequency will return to the point where the threshold can be reached, and comb teeth are generated. Then the state of the system comes back to process (i) and the oscillation will repeat steadily. We examine the frequency shift and oscillation period change under different pump powers, as shown in Figs. 3(e)–3(f). We find that the frequency shift varied from 1 to 7 MHz, while the oscillation period increased from 0.4 to 1.7 s with increasing pump power. This phenomenon is due to the different heating rates of the YIG sphere with varying pump power, which agrees well with the numerical calculations. Furthermore, the Kerr effect in our system is also discussed within the Supplemental Material [45].

As the stabilization and control of the magnonic frequency comb are critical for the potential application of high-precision magnonic frequency spectroscopy, here, we also demonstrate the stabilization and control of the frequency spacing of the magnonic frequency comb via injection locking [44], which significantly suppresses the instability of the comb teeth, as shown in Fig. 4(a). An

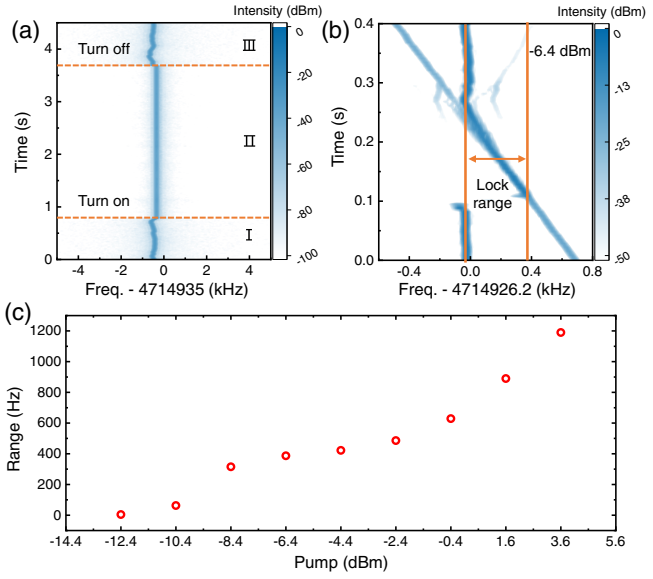

FIG. 4. (a) Evolution of one comb tooth when the external source is on and off. The initial comb tooth is unstable (I). The comb tooth is synchronized to the external source (II). The comb tooth returns to the initial state after turning off the external source (III). (b) Evolution of the rf spectrum with varied injected frequency. The injected power is −6.4 dBm, and the comb is synchronized to the external source when the frequency difference is less than 400 Hz. (c) Locking ranges with varied pump power.

additional source is injected into the YIG microsphere at a frequency of 4.71492 GHz. Prior to turning on the external source, the magnonic frequency comb is generated, and the comb tooth on the rf spectrum is unstable (stage I), particularly when focusing on the comb line at 4.714 92 GHz. We then turn on the external source, and the stabilization of the magnonic frequency comb is notably improved (stage II). Finally, by turning off the external source, the stable comb tooth immediately returns to the initial state and becomes as unstable as before (stage III). Furthermore, we study the locking range of this injection locking scheme. Figure 4(b) displays the evolution of the rf spectra with a power of −6.4 dBm when the external source frequency slowly varied. Initially, when the frequency difference between the external source and comb line is relatively large, beat notes of the initial frequency and external source frequency and their harmonic components all exist in the rf spectrum. As we continue scanning, the comb is injection locked by the external source when their frequency difference is very close. Scanning in the same direction further led to the external source frequency crossing the comb line and going out of the locking range at last. The locking range increases with the enhancement of the external source power, up to a maximum of 1.2 kHz, as depicted in Fig. 4(c).

Discussion.—In conclusion, we demonstrate a magnonic frequency comb in the magnomechanical resonator. The magnonic frequency comb has up to 20 comb lines and a frequency spacing 10.08 MHz, equaling the resonant frequency of the mechanical mode. Additionally, we study the thermal effect involved in the frequency comb generation process, where the frequency comb exhibits periodic oscillations that are dependent on pump power. Our experimental results are in agreement with numerical calculations. Furthermore, we demonstrate the stabilization and control of the frequency spacing of the magnonic frequency comb via injection locking. We can achieve tuning of comb teeth beyond a range of 1 kHz. Our Letter not only advances the study of nonlinear physics in magnonic systems but also unlocks the potential of magnonic frequency combs for sensing and metrology.

The authors thank C.-L. Zou for helpful discussions and suggestions. The work was supported by the National Key Research and Development Program (Grant No. 2020YFB2205801) and National Natural Science Foundation of China (Grants No. 12293052, No. 12293050, No. 11934012, No. 92050109, No. 12104442, and No. 92250302), Innovation program for Quantum Science and Technology (2021ZD0303203), the CAS Project for Young Scientists in Basic Research (YSBR-069), and the Fundamental Research Funds for the Central Universities. This work was partially carried out at the USTC Center for Micro and Nanoscale Research and Fabrication.

*These authors contributed equally to this work.
†shenzhen@ustc.edu.cn
‡chunhua@ustc.edu.cn

[1] T. J. Kippenberg, R. Holzwarth, and S. A. Diddams, Microresonator-based optical frequency combs, Science **332**, 555 (2011).
[2] T. J. Kippenberg, A. L. Gaeta, M. Lipson, and M. L. Gorodetsky, Dissipative kerr solitons in optical microresonators, Science **361**, eaan8083 (2018).
[3] S. A. Diddams, K. Vahala, and T. Udem, Optical frequency combs: Coherently uniting the electromagnetic spectrum, Science **369**, eaay3676 (2020).
[4] Z. L. Newman, V. Maurice, T. Drake, J. R. Stone, T. C. Briles, D. T. Spencer, C. Fredrick, Q. Li, D. Westly, B. R. Ilic *et al.*, Architecture for the photonic integration of an optical atomic clock, Optica **6**, 680 (2019).
[5] M.-G. Suh and K. J. Vahala, Soliton microcomb range measurement, Science **359**, 884 (2018).
[6] P. Trocha, M. Karpov, D. Ganin, M. H. Pfeiffer, A. Kordts, S. Wolf, J. Krockenberger, P. Marin-Palomo, C. Weimann, S. Randel *et al.*, Ultrafast optical ranging using microresonator soliton frequency combs, Science **359**, 887 (2018).
[7] J. Wang, Z. Lu, W. Wang, F. Zhang, J. Chen, Y. Wang, J. Zheng, S. T. Chu, W. Zhao, B. E. Little *et al.*, Long-distance ranging with high precision using a soliton microcomb, Photonics Res. **8**, 1964 (2020).
[8] W. Liang, D. Eliyahu, V. S. Ilchenko, A. A. Savchenkov, A. B. Matsko, D. Seidel, and L. Maleki, High spectral purity Kerr frequency comb radio frequency photonic oscillator, Nat. Commun. **6**, 7957 (2015).
[9] E. Lucas, P. Brochard, R. Bouchand, S. Schilt, T. Südmeyer, and T. J. Kippenberg, Ultralow-noise photonic microwave synthesis using a soliton microcomb-based transfer oscillator, Nat. Commun. **11**, 374 (2020).
[10] J. Liu, E. Lucas, A. S. Raja, J. He, J. Riemensberger, R. N. Wang, M. Karpov, H. Guo, R. Bouchand, and T. J. Kippenberg, Photonic microwave generation in the x-and k-band using integrated soliton microcombs, Nat. Photonics **14**, 486 (2020).
[11] P. Marin-Palomo, J. N. Kemal, M. Karpov, A. Kordts, J. Pfeifle, M. H. Pfeiffer, P. Trocha, S. Wolf, V. Brasch, M. H. Anderson *et al.*, Microresonator-based solitons for massively parallel coherent optical communications, Nature (London) **546**, 274 (2017).
[12] B. Corcoran, M. Tan, X. Xu, A. Boes, J. Wu, T. G. Nguyen, S. T. Chu, B. E. Little, R. Morandotti, A. Mitchell *et al.*, Ultra-dense optical data transmission over standard fibre with a single chip source, Nat. Commun. **11**, 2568 (2020).
[13] F.-X. Wang, W. Wang, R. Niu, X. Wang, C.-L. Zou, C.-H. Dong, B. E. Little, S. T. Chu, H. Liu, P. Hao *et al.*, Quantum key distribution with on-chip dissipative Kerr soliton, Laser Photonics Rev. **14**, 1900190 (2020).
[14] M.-G. Suh, Q.-F. Yang, K. Y. Yang, X. Yi, and K. J. Vahala, Microresonator soliton dual-comb spectroscopy, Science **354**, 600 (2016).
[15] M. Yu, Y. Okawachi, A. G. Griffith, N. Picqué, M. Lipson, and A. L. Gaeta, Silicon-chip-based mid-infrared dual-comb spectroscopy, Nat. Commun. **9**, 1869 (2018).

[16] Q.-F. Yang, B. Shen, H. Wang, M. Tran, Z. Zhang, K. Y. Yang, L. Wu, C. Bao, J. Bowers, A. Yariv *et al.*, Vernier spectrometer using counterpropagating soliton microcombs, Science **363**, 965 (2019).
[17] R. Niu, M. Li, S. Wan, Y. R. Sun, S.-M. Hu, C.-L. Zou, G.-C. Guo, and C.-H. Dong, khz-precision wavemeter based on reconfigurable microsoliton, Nat. Commun. **14**, 169 (2023).
[18] X. Ji, X. Yao, A. Klenner, Y. Gan, A. L. Gaeta, C. P. Hendon, and M. Lipson, Chip-based frequency comb sources for optical coherence tomography, Opt. Express **27**, 19896 (2019).
[19] P. J. Marchand, J. Riemensberger, J. C. Skehan, J.-J. Ho, M. H. Pfeiffer, J. Liu, C. Hauger, T. Lasser, and T. J. Kippenberg, Soliton microcomb based spectral domain optical coherence tomography, Nat. Commun. **12**, 427 (2021).
[20] D. Zhu, C. Chen, M. Yu, L. Shao, Y. Hu, C. Xin, M. Yeh, S. Ghosh, L. He, C. Reimer *et al.*, Spectral control of non-classical light pulses using an integrated thin-film lithium niobate modulator, Light **11**, 327 (2022).
[21] M. Zhang, B. Buscaino, C. Wang, A. Shams-Ansari, C. Reimer, R. Zhu, J. M. Kahn, and M. Lončar, Broadband electro-optic frequency comb generation in a lithium niobate microring resonator, Nature (London) **568**, 373 (2019).
[22] L. S. Cao, D. X. Qi, R. W. Peng, M. Wang, and P. Schmelcher, Phononic frequency combs through nonlinear resonances, Phys. Rev. Lett. **112**, 075505 (2014).
[23] M. H. de Jong, A. Ganesan, A. Cupertino, S. Gröblacher, and R. A. Norte, Mechanical overtone frequency combs, Nat. Commun. **14**, 1458 (2023).
[24] A. Ganesan, C. Do, and A. Seshia, Phononic frequency comb via intrinsic three-wave mixing, Phys. Rev. Lett. **118**, 033903 (2017).
[25] M.-A. Miri, G. DAguanno, and A. Alù, Optomechanical frequency combs, New J. Phys. **20**, 043013 (2018).
[26] Y. Hu, S. Ding, Y. Qin, J. Gu, W. Wan, M. Xiao, and X. Jiang, Generation of optical frequency comb via giant optomechanical oscillation, Phys. Rev. Lett. **127**, 134301 (2021).
[27] J. Zhang, B. Peng, S. Kim, F. Monifi, X. Jiang, Y. Li, P. Yu, L. Liu, Y.-x. Liu, A. Alù *et al.*, Optomechanical dissipative solitons, Nature (London) **600**, 75 (2021).
[28] A. Serga, A. Chumak, and B. Hillebrands, YIG magnonics, J. Phys. D **43**, 264002 (2010).
[29] B. Lenk, H. Ulrichs, F. Garbs, and M. Münzenberg, The building blocks of magnonics, Phys. Rep. **507**, 107 (2011).
[30] Z.-X. Liu, C. You, B. Wang, H. Xiong, and Y. Wu, Phase-mediated magnon chaos-order transition in cavity opto-magnonics, Opt. Lett. **44**, 507 (2019).
[31] H. Wang, J. Chen, T. Liu, J. Zhang, K. Baumgaertl, C. Guo, Y. Li, C. Liu, P. Che, S. Tu *et al.*, Chiral spin-wave velocities induced by all-garnet interfacial Dzyaloshinskii-Moriya interaction in ultrathin yttrium iron garnet films, Phys. Rev. Lett. **124**, 027203 (2020).
[32] C.-Z. Chai, Z. Shen, Y.-L. Zhang, H.-Q. Zhao, G.-C. Guo, C.-L. Zou, and C.-H. Dong, Single-sideband microwave-to-optical conversion in high-q ferrimagnetic microspheres, Photonics Res. **10**, 820 (2022).
[33] Z. Shen, G.-T. Xu, M. Zhang, Y.-L. Zhang, Y. Wang, C.-Z. Chai, C.-L. Zou, G.-C. Guo, and C.-H. Dong, Coherent coupling between phonons, magnons, and photons, Phys. Rev. Lett. **129**, 243601 (2022).
[34] Y.-P. Wang, G. Q. Zhang, D. Zhang, T. F. Li, C. M. Hu, and J. Q. You, Bistability of cavity magnon polaritons, Phys. Rev. Lett. **120**, 057202 (2018).
[35] J. W. Rao, B. Yao, C. Y. Wang, C. Zhang, T. Yu, and W. Lu, Unveiling a pump-induced magnon mode via its strong interaction with walker modes, Phys. Rev. Lett. **130**, 046705 (2023).
[36] Z. Wang, H. Y. Yuan, Y. Cao, Z. X. Li, R. A. Duine, and P. Yan, Magnonic frequency comb through nonlinear magnon-skyrmion scattering, Phys. Rev. Lett. **127**, 037202 (2021).
[37] Z. Wang, H. Y. Yuan, Y. Cao, and P. Yan, Twisted magnon frequency comb and Penrose superradiance, Phys. Rev. Lett. **129**, 107203 (2022).
[38] Z.-X. Liu and Y.-Q. Li, Optomagnonic frequency combs, Photonics Res. **10**, 2786 (2022).
[39] X. Zhang, C.-L. Zou, L. Jiang, and H. X. Tang, Cavity magnomechanics, Sci. Adv. **2**, e1501286 (2016).
[40] R. C. Shen, J. Li, Z. Y. Fan, Y. P. Wang, and J. Q. You, Mechanical bistability in Kerr-modified cavity magnomechanics, Phys. Rev. Lett. **129**, 123601 (2022).
[41] C. A. Potts, E. Varga, V. A. S. V. Bittencourt, S. Viola Kusminskiy, and J. P. Davis, Dynamical backaction magnomechanics, Phys. Rev. X **11**, 031053 (2021).
[42] J. Li, S. Y. Zhu, and G. S. Agarwal, Magnon-photon-phonon entanglement in cavity magnomechanics, Phys. Rev. Lett. **121**, 203601 (2018).
[43] H. Xiong, Magnonic frequency combs based on the resonantly enhanced magnetostrictive effect, Fundam. Res. **3**, 8 (2023).
[44] S. Wan, R. Niu, Z.-Y. Wang, J.-L. Peng, M. Li, J. Li, G.-C. Guo, C.-L. Zou, and C.-H. Dong, Frequency stabilization and tuning of breathing solitons in Si_3N_4 microresonators, Photonics Res. **8**, 1342 (2020).
[45] See Supplemental Material at http://link.aps.org/supplemental/10.1103/PhysRevLett.131.243601 for more details about theory.
[46] G.-T. Xu, M. Zhang, Z.-Y. Wang, Y. Wang, Y.-X. Liu, Z. Shen, G.-C. Guo, and C.-H. Dong, Ringing spectroscopy in the magnomechanical system, Fundam. Res. **3**, 45 (2023).
[47] T. Carmon, L. Yang, and K. J. Vahala, Dynamical thermal behavior and thermal self-stability of microcavities, Opt. Express **12**, 4742 (2004).